Bulletin of the Seismological Society of America, Vol. 107, No. 2, pp. –, April 2017, doi: 10.1785/0120160251

Short Note

The Relation between Ground Acceleration and Earthquake Source Parameters: Theory and Observations

by Itzhak Lior and Alon Ziv

Abstract A simple relation between the root mean square (rms) of the ground acceleration and earthquake spectral (or source) parameters is introduced:

$$A_{\mathrm{rms}} = (2\pi)^2 \Omega_0 \frac{f_0^2}{\sqrt{\pi\kappa T}\left(1 + \frac{\pi\kappa f_0}{1.5^{0.25}}\right)^2},$$

in which Ω_0 is the low-frequency displacement spectral plateau, f_0 is the corner frequency, κ is an attenuation parameter, and T is the data interval. This result uses the omega-square model for far-field radiation and accounts for site-specific attenuation. The main advantage of the new relation with respect to that of Hanks (1979) is that it relaxes the simplifying assumption that the spectral corner frequency is much smaller than the maximum corner frequency resulting from attenuation, and that the spectrum may be approximated as being perfectly flat between the two frequencies. The newly proposed relation is tested using a composite dataset of earthquake records from Japan, California, Mexico, and Taiwan. Excellent agreement is found between observed and predicted ground acceleration for any combination of corner frequencies. Thus, use of the above relation enables the extrapolation of ground-motion prediction equation inferred from the frequent small-magnitude earthquakes to the rare large magnitudes. This capacity is extremely useful near slow-slip plate boundaries, where the seismic moment release rates are low.

Introduction

Understanding how ground motion depends on earthquake source parameters is of interest to both earthquake seismologists and earthquake engineers. The former can use this understanding to constrain source parameters (e.g., Baltay *et al.*, 2013; Lior *et al.*, 2016), and the latter may incorporate it into ground-motion prediction equations that are key ingredients in any seismic-hazard assessment (e.g., Boore and Atkinson, 2008; Campbell and Bozorgnia, 2008; Abrahamson *et al.*, 2014). A commonly utilized relation between ground acceleration and source parameters is

$$A_{\mathrm{rms}}^{\mathrm{MH}} = \frac{(2\pi)^2 \Delta\tau}{106\rho R} \sqrt{\frac{f_{\max}}{f_0}} \tag{1}$$

(Hanks, 1979; McGuire and Hanks, 1980), in which A_{rms} is the ground acceleration root mean square (rms), with the superscript referring to McGuire and Hanks (1980), $\Delta\tau$ is the stress drop, f_0 is the corner frequency, and $f_{\max}$ is the frequency above which the acceleration spectrum drops steeply (Hanks, 1982). As several approximations were made throughout the derivation of this expression, it is instructive to revisit this result and assess the extent to which relaxing the simplifying assumptions underlying its derivation improves ground acceleration prediction.

In this study, an exact solution for A_{rms} is obtained. Owing to its complex form, an analytical approximation to the exact solution is provided. Finally, the performance of the newly derived A_{rms} prediction is compared with previous results (Hanks, 1979; McGuire and Hanks, 1980; Hanks and McGuire, 1981), using a composite dataset of earthquake records from Japan, California, Mexico, and Taiwan. Next, for the sake of completeness, the approach leading to equation (1) is described, and the various approximations and simplifying assumptions that enter its derivation are stated.

The Simplifying Assumptions Underlying $A_{\mathrm{rms}}^{\mathrm{MH}}$

The point of departure in the derivation of equation (1) is Brune's earthquake source model (Brune, 1970), according to which the far-field spectral amplitude of the ground acceleration reads as

$$\ddot{\Omega}(f) = (2\pi f)^2 \frac{\Omega_0}{1 + (\frac{f}{f_0})^2}, \quad (2)$$

in which f is the frequency, f_0 is the corner frequency, and Ω_0 is the spectral plateau of the low-frequency displacement spectrum. The two spectral parameters Ω_0 and f_0 hold fundamental information regarding the physical attributes of the earthquake source. The former is a function of the seismic moment and the hypocentral distance according to

$$\Omega_0 = \frac{M_0 U_{\varphi\theta} F_s}{4\pi\rho C_S^3 R}, \quad (3)$$

with $U_{\varphi\theta}$ being the radiation pattern, F_s being a free-surface correction factor, C_S being the S-wave velocity, R being the hypocentral distance, and ρ being the density. The corner frequency is related to the stress drop and the seismic moment as

$$f_0 = kC_s \left(\frac{16}{7}\frac{\Delta\tau}{M_0}\right)^{1/3}, \quad (4)$$

with k being a constant. From equation (2), the acceleration spectral amplitude increases as f^2 at frequencies below the corner frequency and approaches asymptotically to $(2\pi f_0)^2\Omega_0$ above it (Fig. 1). In practice, however, the acceleration spectral plateau is attenuated due to anelastic and near-site effects (dotted line in Fig. 1), and is truncated by the Nyquist frequency. While for local earthquakes, the effect of the distance-dependent anelastic attenuation is usually minor (Wu *et al.*, 2005; Wu and Zhao, 2006; Lior *et al.*, 2016), that of the near-site attenuation is not. The spectral amplitude subject to site-specific attenuation may be expressed as

$$\ddot{\Omega}(f) = (2\pi f)^2 \frac{\Omega_0}{1 + (\frac{f}{f_0})^2} \exp(-\pi\kappa f), \quad (5)$$

in which κ is a site-specific attenuation parameter (Anderson and Hough, 1984). This attenuation introduces an additional corner frequency that is hereafter referred to as f_κ:

$$f_\kappa = \frac{1}{\pi\kappa} \quad (6)$$

(Hanks, 1979). The rms of the ground-motion acceleration may be obtained by inserting the ground acceleration spectrum $\ddot{\Omega}(f)$ into Parseval's theorem:

$$A_{\mathrm{rms}} = \sqrt{\frac{\int_{-\infty}^{\infty} |\ddot{\Omega}(f)|^2 df}{T}}, \quad (7)$$

with T being the data interval. From this point onward, Hanks (1979) and McGuire and Hanks (1980) disregarded the possibility that f_0 could be larger than f_κ. By setting f_κ to be equal to $f_{\max}$, and approximating the acceleration spectrum as being equal to $(2\pi f_0)^2\Omega_0$ between f_0 and $f_{\max}$ (thick black line in Fig. 1), they obtained

$$A_{\mathrm{rms}}^{\mathrm{MH1}} = (2\pi)^2\Omega_0 \frac{f_0^{2.5}}{\sqrt{T}} \sqrt{\frac{f_{\max}}{f_0} - 1}, \quad (8)$$

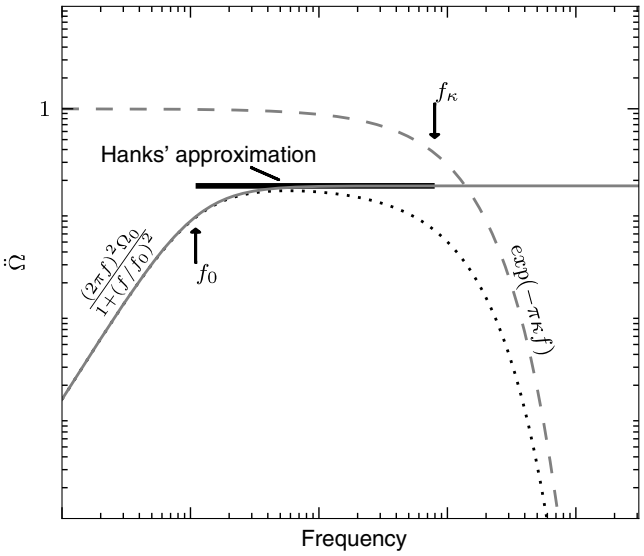

Figure 1. Schematic diagram illustrating the effect of near-site attenuation on the acceleration spectra. The omega-square model and the near-site attenuation are indicated by solid and dashed gray lines, respectively, and the acceleration spectrum subject to near-site attenuation is indicated by a dotted line. The horizontal thick black line between f_0 and f_κ represents Hanks' approximation (Hanks, 1979).

in which MH1 stands for McGuire and Hanks' first set of approximations. For most moderate-to-large earthquakes, it is expected that $f_{\max}$ will be much larger than f_0, in which case the above expression may be further simplified as

$$A_{\mathrm{rms}}^{\mathrm{MH2}} = (2\pi)^2\Omega_0 \frac{f_0^{2.5}}{\sqrt{T}} \sqrt{\frac{f_{\max}}{f_0}}, \quad (9)$$

in which MH2 signifies McGuire and Hanks' additional approximation, namely $f_{\max} \gg f_0$. Further setting the data interval to be equal to the rupture duration, $1/f_0$, and substituting equations (3) and (4) into equation (9) leads to equation (1).

In summary, equation (1) is model based (Brune, 1970), and rests on two simplifying assumptions: (1) $f_{\max} \gg f_0$, and (2) the spectrum may be approximated as being equal to $(2\pi f_0)^2\Omega_0$ between f_0 and $f_{\max}$. Hanks and McGuire (1981) further assumed that the peak ground acceleration (PGA) occurs within $1/f_0$ from the time of the first S-wave arrival, and related A_{rms} to PGA.

Exact Solution and Analytical Approximation for A_{rms}

The exact solution for A_{rms} is obtained via insertion of $\ddot{\Omega}(f)$ (equation 5) into equation (7) as follows:

$$A_{\mathrm{rms}}^{\mathrm{exact}} = (2\pi)^2\Omega_0 \sqrt{\frac{2}{T}\int_0^\infty \frac{f^4}{(1 + (\frac{f}{f_0})^2)^2} \exp(-2\pi\kappa f) df}. \quad (10)$$

The solution of the above integral is

$$A_{\mathrm{rms}}^{\mathrm{exact}}=(2\pi)^2\Omega_0\frac{1}{\sqrt{2T}(\pi\kappa)^{2.5}}\alpha_0^2\sqrt{2-2\alpha_0 Ci(2\alpha_0)[2\alpha_0\cos(2\alpha_0)+3\sin(2\alpha_0)]+[\pi\alpha_0-2\alpha_0 Si(2\alpha_0)][2\alpha_0\sin(2\alpha_0)-3\cos(2\alpha_0)]} \tag{11}$$

(corrected equation A3 of Luco, 1985), with $\alpha_0 = \pi\kappa f_0 = f_0/f_\kappa$, and Ci and Si being the cosine integral function and the sine integral function, respectively. For $\alpha_0 \to 0$, the situation considered in Hanks (1979), the rms of the ground acceleration is asymptotic to $(2\pi)^2\Omega_0\alpha_0^2/(\sqrt{T}(\pi\kappa)^{2.5})$. Whereas for $\alpha_0 \to \infty$, the ground acceleration intensity is independent of f_0 and is asymptotic to $(2\pi)^2\Omega_0\sqrt{1.5}/(\sqrt{T}(\pi\kappa)^{2.5})$. Given the complex form of the above result, it is sensible to seek a simpler expression. An analytical approximation that satisfies the two asymptotic solutions is

$$A_{\mathrm{rms}}^{\sim\mathrm{exact}} = (2\pi)^2\Omega_0\frac{\alpha_0^2}{\sqrt{T}(\pi\kappa)^{2.5}(1+\frac{\alpha_0}{1.5^{0.25}})^2}, \tag{12a}$$

or equivalently

$$A_{\mathrm{rms}}^{\sim\mathrm{exact}} = (2\pi)^2\Omega_0\frac{f_0^2}{\sqrt{\pi\kappa T}(1+\frac{\pi\kappa f_0}{1.5^{0.25}})^2}, \tag{12b}$$

with the ∼exact signifying analytically approximated exact solution. Inspection of normalized A_{rms} as a function of α_0 (Fig. 2) reveals an excellent agreement between the exact and the analytically approximated solution when f_0 is much larger than or much smaller than f_κ, and a maximum misfit of 6.5% when $f_0 \sim f_\kappa$. The agreement between the exact solution and the two approximate solutions, MH1 (equation 8) and MH2 (equation 9), is excellent when $f_0 \ll f_\kappa$ (i.e., $\alpha_0 \to 0$), and that with MH1 is still quite good when $f_0 \sim f_\kappa$. Beyond their range of validity, in which $f_0 \geq f_\kappa$ (i.e., $\alpha_0 > 1$), MH2 diverges rapidly from the exact solution, and MH1 becomes imaginary.

Finally, substituting equations (3) and (4) into (12b) yields an equivalent expression for $A_{\mathrm{rms}}^{\sim\mathrm{exact}}$ in terms of the seismic moment, the stress drop, and the hypocentral distance as

$$A_{\mathrm{rms}}^{\sim\mathrm{exact}} = \beta\frac{M_0^{1/3}\Delta\tau^{2/3}}{\sqrt{\kappa T}R}/(1+1.5^{-0.25}\pi\kappa k C_S\left(\frac{16\Delta\tau}{7M_0}\right)^{1/3})^2, \tag{13}$$

in which $\beta = 4\pi U_{\phi\theta}Fs(16/7)^{2/3}(kC_S)^2/(\sqrt{\pi}4\rho C_S^3)$. In the next section, the goodness of the $A_{\mathrm{rms}}^{\sim\mathrm{exact}}$ prediction is compared with that of $A_{\mathrm{rms}}^{\mathrm{MH1}}$ and $A_{\mathrm{rms}}^{\mathrm{MH2}}$ using a composite dataset of earthquake records.

Data and Analysis

The Composite Catalog

The dataset used in this study (Fig. 3) consists of 6311 three-component seismograms, with signal-to-noise ratio that is greater than 20 and whose hypocentral distances are less than 60 km. It includes 3042 velocity seismograms and 286 accelerograms recorded by the California Integrated Seismic Network, 2917 accelerograms recorded by Japan's K-NET and KiK-net surface accelerometers, and 66 accelerograms from the Pacific Earthquake Engineering Research–Next Generation Attenuation of Ground Motions (PEER NGA) database (Ancheta *et al.*, 2014). These data are associated with 542 southern California earthquakes whose magnitude is between 3 and 6, 196 Japan earthquakes whose magnitude is between 4 and 7.3, the 1999 M_{w} 7.6 Chi-Chi earthquake, and the 2010 M_{w} 7.2 El Mayor–Cucapah earthquake. *P*-phase arrivals were picked manually, zero-offset corrections were applied, and acceleration time series were high-pass filtered at 0.02 Hz. The rms of the ground acceleration A_{rms} is calculated according to $\sqrt{\sum_{i=1}^{n}[\mathrm{AZ}_i^2+\mathrm{AE}_i^2+\mathrm{AN}_i^2]/n}$, in which AZ, AE, and AN are the acceleration amplitudes along the vertical, east, and north directions, respectively, and n is the number of samples within the data interval. The start and end times of the data intervals were determined with the objective of including the direct *S* waves that are emitted from the source, while excluding, as much as possible, the weaker coda waves that follow. With this in mind, the start time of the data interval is set to be equal to the first *S*-wave arrival $T_{\mathrm{start}} = T_P + R/8$, with T_P being the time of the first *P*-phase arrival and R being the hypocentral distance (in kilometers, derived from the earthquake catalog); the duration of the data interval is set to be equal to the sum of the *S*-wave travel time and the rupture duration $T_{\mathrm{end}} - T_{\mathrm{start}} = R/C_S + 1/f_0$, with C_S being an average *S*-wave velocity of 3.2 km/s, and the corner frequency is estimated from equation (4) using a stress drop of 1 MPa (later, the corner frequency will be obtained through spectral inversion). Thus, the data interval of small earthquakes (i.e., short rupture durations) ends approximately when the elapsed time since the earthquake origin time is twice the *S*-wave travel time, which according to coda-wave studies marks the onset of coda waves (Rautian and Khalturin, 1978; Herraiz and Espinosa, 1987). The addition of the distance-dependent term R/C_S to the data interval accounts for the increase of the wave-packet spread with distance from the earthquake source (Boore and Thompson, 2014).

Modeling κ, f_0, and Ω_0

The spectral parameters κ, f_0, and Ω_0 are obtained in two steps. First, κ is modeled by fitting the high-frequency portion of the acceleration spectra to

$$\ln(A(f)) = a - \pi\kappa f; \qquad 10\ \mathrm{Hz} < f < 25\ \mathrm{Hz}, \tag{14}$$

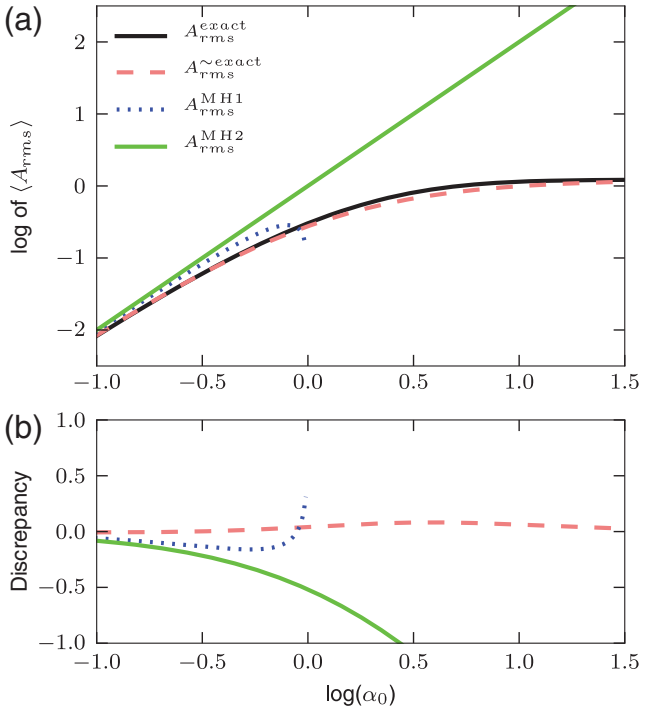

Figure 2. Comparison between $A_{\rm rms}^{\rm exact}$ and the three approximate solutions $A_{\rm rms}^{\sim\rm exact}$, $A_{\rm rms}^{\rm MH1}$, and $A_{\rm rms}^{\rm MH2}$ ($A_{\rm rms}$ is the ground acceleration root mean square [rms], MH1 is the McGuire and Hanks (1980) first set of approximations, and MH2 signifies McGuire and Hanks' additional approximation). (a) The logarithm of normalized $A_{\rm rms}$, $\langle A_{\rm rms}\rangle = A_{\rm rms}\sqrt{T}(\pi\kappa)^{2.5}/((2\pi)^2\Omega_0)$, as a function of the logarithm of α_0. (b) Discrepancy between the logarithm of $A_{\rm rms}^{\rm exact}$ and $A_{\rm rms}^{\sim\rm exact}$, $A_{\rm rms}^{\rm MH1}$, and $A_{\rm rms}^{\rm MH2}$, as a function of the logarithm of α_0.

with $A(f)$ being the spectral amplitudes, and a and κ being the fitting parameters (Anderson and Hough, 1984). The fit to the above function is done for frequencies between 10 and 25 Hz (Oth *et al.*, 2011). The distribution of individual records and station-average κ are shown in Figure 4a. Average κ for California and Japan are similar and equal to 0.04 s. This κ distribution is similar to previously reported distributions from California, Japan, and Taiwan (Oth *et al.*, 2011; Van Houtte *et al.*, 2011).

After having determined κ, the remaining spectral parameters f_0 and Ω_0 are determined via grid-search approach, with the objective function being the absolute difference between the logarithm of the observed spectra and the logarithm of the attenuated Brune's predicted spectra (equation 5), with κ set to be equal to the individual record value obtained in the previous step. This approach is equivalent to solving f_0 and Ω_0 using equation (2) and the κ-corrected spectra. Furthermore, because here κ is determined per seismogram, it embodies both site and path effects (Anderson and Hough, 1984). The above analysis indicates that the f_0 to f_κ ratio of most of the $M_{\rm w}$ <5 and about 50% of the $5 \le M_{\rm w} < 6.5$ are inconsistent with the MH2 approximation (Fig. 4b).

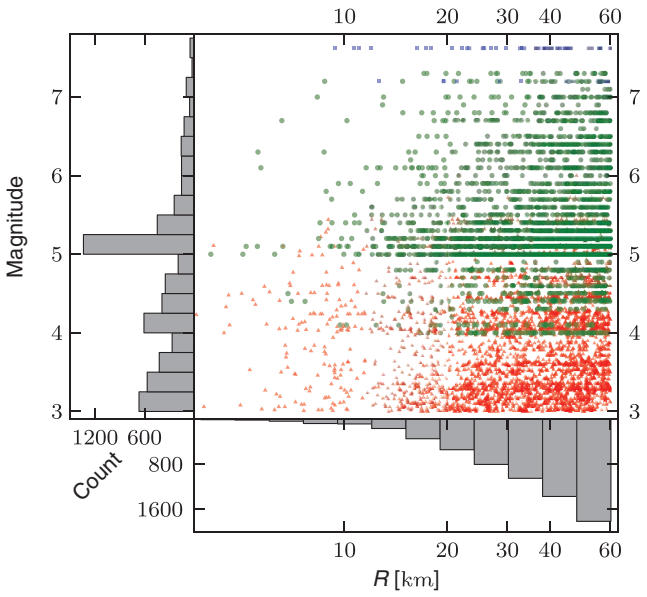

Figure 3. Waveform distribution according to magnitude and hypocentral distances derived from the earthquake catalogs. Red triangles indicate seismograms recorded by the California Integrated Seismic Network, green circles indicate accelerograms recorded by the K-NET and KiK-net surface accelerometers, and blue squares indicate accelerograms from the Pacific Earthquake Engineering Research–Next Generation Attenuation of Ground Motions (PEER NGA) database associated with two earthquakes from Taiwan and Mexico.

Comparison between Observed and Predicted $A_{\rm rms}$

The performances of $A_{\rm rms}^{\sim\rm exact}$ and $A_{\rm rms}^{\rm MH2}$ predictions are compared in Figure 5. Similar comparison with $A_{\rm rms}^{\rm exact}$ is not shown, because it is not visually distinguishable from $A_{\rm rms}^{\sim\rm exact}$. A comparison with $A_{\rm rms}^{\rm MH1}$ is not shown either, because this expression is mathematically restricted to $f_0 < f_\kappa$, and thus cannot be directly compared with the others. The standard deviations of the discrepancies between observed and predicted $A_{\rm rms}$ (reported at the top panels of Fig. 5) indicate that $A_{\rm rms}^{\sim\rm exact}$ exhibits smaller discrepancies than $A_{\rm rms}^{\rm MH2}$. Inspection of these discrepancies as a function of α_0 reveals similarly good agreement between observed and predicted $A_{\rm rms}$ for the two predictions when $f_0 \ll f_\kappa$. Not surprisingly, the discrepancy between the observed and the MH2-predicted $A_{\rm rms}$ is α_0 dependent, and the prediction of $A_{\rm rms}^{\rm MH2}$ becomes less reliable with increasing α_0 beyond ~0.1. In contrast, the discrepancy between the observed and the ~exact-predicted $A_{\rm rms}$ remains fairly small when the small corner-frequency condition is not met. Thus, the robustness of $A_{\rm rms}^{\sim\rm exact}$ for ground-motion prediction for all α_0 values is established. It must be emphasized that the MH solutions were never intended to apply for $f_0 > f_\kappa$, and the observed behavior is as expected.

PGA–$A_{\rm rms}$ Relation

The PGA is a key parameter in earthquake-hazard analyses, design of building codes, algorithms for earthquake early

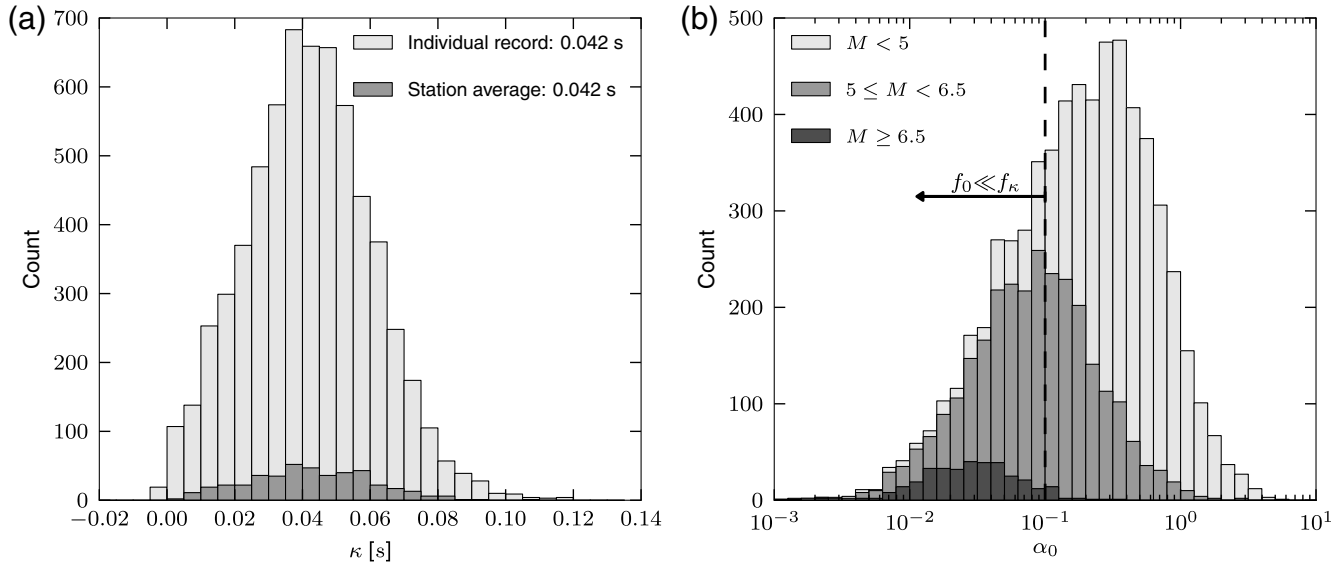

Figure 4. Histograms showing the distribution of κ and α_0. (a) The distributions of record-specific and station-average κ values are indicated in light and dark gray, respectively. (b) The distribution of α_0 according to magnitude bins. The area left of the vertical dashed line indicates the region where the $f_0 \ll f_\kappa$ approximation is valid.

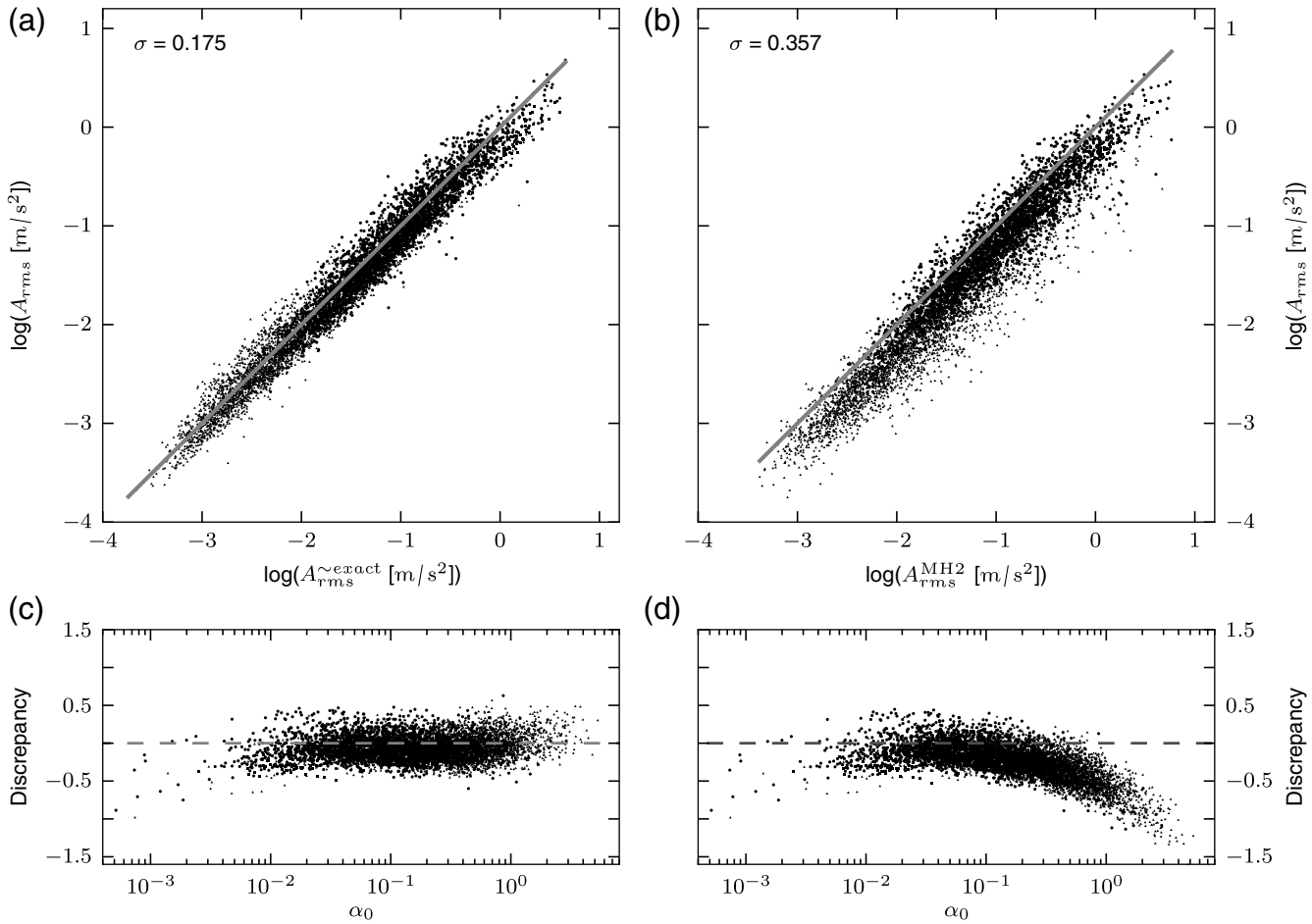

Figure 5. Observed versus predicted $A_{\rm rms}$. (a) The logarithm of observed $A_{\rm rms}$ as a function of the logarithms of $A_{\rm rms}^{\sim \rm exact}$. (b) The logarithm of observed $A_{\rm rms}$ as a function of the logarithms of $A_{\rm rms}^{\rm MH2}$. (c) $\log(A_{\rm rms}) - \log(A_{\rm rms}^{\sim \rm exact})$ as functions of α_0. (d) $\log(A_{\rm rms}) - \log(A_{\rm rms}^{\rm MH2})$ as functions of α_0.

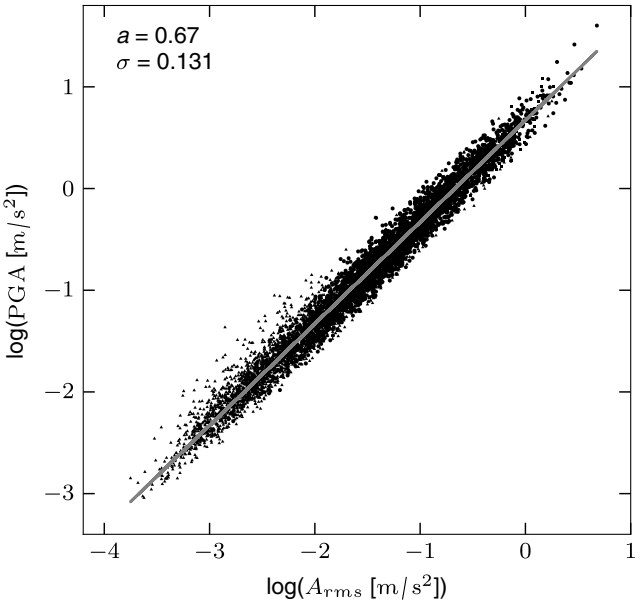

Figure 6. The logarithm of peak ground acceleration (PGA) as a function of the logarithm of acceleration root mean square. The gray line indicates a linear regression to $\log(\mathrm{PGA}) = a + \log(A_{\mathrm{rms}})$, the fitting coefficient a, and standard deviation are reported at the top left corner.

warning, and more. Thus, it is instructive to establish a relation between PGA and A_{rms}. Hanks and McGuire (1981) obtained the following equation:

$$\frac{\mathrm{PGA}}{A_{\mathrm{rms}}} = \sqrt{2\ln\left(\frac{2f_{\mathrm{max}}}{f_0}\right)}. \qquad (15)$$

The above relation has been validated against large datasets (e.g., Baltay *et al.*, 2013), including the data used in this study (not shown). Yet, because it is mathematically restricted to $f_0 < 2f_{\mathrm{max}}$, it is useful to establish a PGA–A_{rms} relation that is assumption free. The log–log diagram of PGA as a function of A_{rms} is shown in Figure 6, with the former calculated according to $\max(\sqrt{\mathrm{AZ}_i^2 + \mathrm{AE}_i^2 + \mathrm{AN}_i^2})$. Regression analysis yields the following scaling:

$$\mathrm{PGA} = 4.7(\pm 1.4)A_{\mathrm{rms}}. \qquad (16)$$

The above empirical relation may be combined with equation (13) to get a ground-motion prediction equation for PGA.

Summary

A simple relation between A_{rms} and source (or spectral) parameters is introduced that is based on Brune's omega-square model for far-field radiation (Brune, 1970). The main advantage of the new relation with respect to the commonly utilized $A_{\mathrm{rms}}^{\mathrm{MH}}$ relation (Hanks, 1979; McGuire and Hanks, 1980) is that it relaxes the simplifying assumption $f_{\mathrm{max}} \gg f_0$ and the assumption that the spectrum may be approximated as being perfectly flat between f_0 and f_{max}.

The prediction of the newly derived relation is compared with that of $A_{\mathrm{rms}}^{\mathrm{MH}}$ using a composite dataset of earthquake records from Japan, California, Mexico, and Taiwan. The spectral parameters κ, f_0, and Ω_0 are obtained in two steps via spectral inversion. On average, the values of κ for California and Japan are similar and are close to 0.04 s (Fig. 4a). The ratio between f_0 and f_κ of most $M_{\mathrm{w}} < 5$ and half of the $5 \le M_{\mathrm{w}} < 6.5$ are inconsistent with the MH2 approximation (Fig. 4b). Thus, use of $A_{\mathrm{rms}}^{\sim\mathrm{exact}}$, whose prediction is nearly independent of α_0, is advantageous.

In summary, the availability of a single formulation that is valid for any value of α_0 provides a powerful tool for ground-motion prediction, as it enables the extrapolation of GMPE inferred from the frequent small-magnitude earthquakes to the rare large magnitudes. This capacity is extremely important near slow-slip plate boundaries, where the seismic moment release rates are low.

Data and Resources

The data used in this study were obtained from the Southern California Earthquake Data Center (Caltech. Dataset, http://scedc.caltech.edu/, last accessed January 2016), the K-NET and KiK-net strong-motion networks (http://www.kyoshin.bosai.go.jp/, last accessed January 2016), and from the Pacific Earthquake Engineering Research (PEER) Ground Motion Database (http://ngawest2.berkeley.edu/site/, last accessed January 2016).

Acknowledgments

We thank Associate Editor Hiroshi Kawase for his work and insightful comments. We also thank two anonymous reviewers for their very constructive remarks. This research was supported by the Ministry of Energy and Water Resources Grant Number 214-17-019.

References

Abrahamson, N. A., W. J. Silva, and R. Kamai (2014). Summary of the ASK14 ground motion relations for active crustal regions, *Earthq. Spectra* **30,** 1025–1055.

Ancheta, T. D., R. B. Darragh, J. P. Stewart, E. Seyhan, W. J. Silva, B. S. J. Chiou, K. E. Wooddell, R. W. Graves, A. R. Kottke, D. M. Boore, *et al.* (2014). NGA-West2 database, *Earthq. Spectra* **30,** 989–1005, doi: 10.1193/070913EQS197M.

Anderson, J. G., and S. E. Hough (1984). A model for the shape of the Fourier amplitude spectrum of acceleration at high frequencies, *Bull. Seismol. Soc. Am.* **74,** 1969–1993.

Baltay, A. S., T. C. Hanks, and G. C. Beroza (2013). Stable stress-drop measurements and their variability: Implications for ground-motion prediction, *Bull. Seismol. Soc. Am.* **103,** 211–222.

Boore, D. M., and G. M. Aktinson (2008). Ground-motion prediction equations for the average horizontal component of PGA, PGV, and 5%-damped PSA at spectral periods between 0.01 s and 10.0 s, *Earthq. Spectra* **24,** 99–138.

Boore, D. M., and E. M. Thompson (2014). Path durations for use in the stochastic-method simulation of ground motions, *Bull. Seismol. Soc. Am.* **104,** 2541–2552.

Brune, J. N. (1970). Tectonic stress and the spectra of seismic shear waves from earthquakes, *J. Geophys. Res.* **75,** 4997–5009.

Campbell, K. W., and Y. Bozorgnia (2008). NGA ground motion model for the geometric mean horizontal component of PGA, PGV, PGD and 5% damped linear elastic response spectra for periods ranging from 0.01 to 10 s, *Earthq. Spectra* **24,** 139–172.

Hanks, T. C. (1979). b values and $\omega^{-\gamma}$ seismic source models: Implications for tectonic stress variations along active crustal fault zones and the estimation of high-frequency strong ground motion, *J. Geophys. Res.* **84,** 2235–2241.

Hanks, T. C. (1982). $f_{\max}$, *Bull. Seismol. Soc. Am.* **72,** 1867–1879.

Hanks, T. C., and R. K. McGuire (1981). The character of high-frequency strong ground motion, *Bull. Seismol. Soc. Am.* **71,** 2071–2095.

Herraiz, M., and F. Espinosa (1987). Coda waves: A review, *Pure Appl. Geophys.* **125,** 499–577.

Lior, I., A. Ziv, and R. Madariaga (2016). *P*-wave attenuation with implications for earthquake early warning, *Bull. Seismol. Soc. Am.* **106,** 13–22, doi: 10.1785/0120150087.

Luco, J. E. (1985). On strong ground motion estimates based on models of the radiated spectrum, *Bull. Seismol. Soc. Am.* **75,** 641–649.

McGuire, R. K., and T. C. Hanks (1980). RMS accelerations and spectral amplitudes of strong ground motion during the San Fernando, California, earthquake, *Bull. Seismol. Soc. Am.* **70,** 1907–1919.

Oth, A., D. Bindi, S. Parolai, and D. D. Giacomo (2011). Spectral analysis of K-NET and KiK-net data in Japan, part II: On attenuation characteristics, source spectra, and site response of borehole and surface stations, *Bull. Seismol. Soc. Am.* **101,** 667–687.

Rautian, T. G., and V. I. Khalturin (1978). The use of the coda for determination of the earthquake source spectrum, *Bull. Seismol. Soc. Am.* **68,** 923–948.

Van Houtte, C., S. Drouet, and F. Cotton (2011). Analysis of the origins of κ (kappa) to compute hard rock to rock adjustment factors for GMPEs, *Bull. Seismol. Soc. Am.* **101,** 2926–2941.

Wu, Y. M., and L. Zhao (2006). Magnitude estimation using the first three seconds *P*-wave amplitude in earthquake early warning, *Geophys. Res. Lett.* **33,** L16312, doi: 10.1029/2006GL026871.

Wu, Y. M., R. M. Allen, and C. F. Wu (2005). Revised M_L determination for crustal earthquakes in Taiwan, *Bull. Seismol. Soc. Am.* **95,** 2517–2524.

Department of Geosciences
Tel-Aviv University
P.O. Box 39040
Tel-Aviv 6997801, Israel
itzhaklior22@gmail.com

Manuscript received 2 August 2016;
Published Online 3 January 2017